Journal of Applied Analysis and Computation
Volume 14, Number 1, February 2024, 61–83
Website:http://www.jaac-online.com
DOI:10.11948/20230018

SPECTRAL-GALERKIN APPROXIMATION BASED ON REDUCED ORDER SCHEME FOR FOURTH ORDER EQUATION AND ITS EIGENVALUE PROBLEM WITH SIMPLY SUPPORTED PLATE BOUNDARY CONDITIONS

Yuanlu Wang[1], Jiantao Jiang[1] and Jing An[1,†]

Abstract We develop in this paper a high-order numerical method for fourth-order equation with simply supported plate boundary conditions in a circular domain. By introducing an auxiliary function and using the dimension reduction technique, we reduce the fourth-order problem to a one-dimensional second-order coupled problem. Based on the one-dimensional second-order coupled problem, we prove the uniqueness of the weak solution and approximation solutions and the error estimation between them. Moreover, we extend the approach to fourth-order eigenvalue problem with simply supported plate boundary conditions in a circular domain. Finally, we carry out some numerical experiments to validate the theoretical analysis and algorithm.

Keywords Fourth-order problems, reduced order scheme, spectral-Galerkin approximation, error estimation.

MSC(2010) 65M15, 65N30.

1. Introduction

Fourth-order problems appear in many mathematical models for scientific and engineering applications, such as the structural and continuum mechanics with applications to thin beams and plates [8,9,14,28], the vibration problems involving various boundary conditions [1,10,11,25], and so on. In addition, the numerical computation of many complex nonlinear problems like Allen-Cahn equation, Cahn-Hilliard equation and transmission eigenvalue problem can also be accomplished by solving a fourth-order equation repeatedly [16,19,23,24,26].

Up to now, there have been various numerical methods for solving fourth-order problems with different boundary conditions in multifarious geometric domain, including finite element methods [5,7,15,27], spectral methods and some high-order numerical methods [2,4,6,12,13,17,18,22]. For finite element methods, the regional division and requirement of C^1 finite element spaces will generate a large num-

[†]The corresponding author.
[1]School of Mathematical Sciences, Guizhou Normal University, Guiyang 550025, China
Email: wy520825@163.com(Y. Wang), rivers2021@163.com(J. Jiang), aj154@163.com(J. An)

ber of degrees of freedom, especially for the fourth-order problems in some special domains similar to circular domain. As we all know, spectral method is a high-order numerical method with spectral accuracy, which plays an important role in solving partial differential equations [21]. However, for some fourth-order problems with simply supported plate boundary conditions in a circular/spherical domain, spectral method can not be directly applied to solve them. Although An et al. can convert a circular or spherical domain into a standard domain by using polar or spherical coordinate transformation, the pole singularity and the complexity of boundary conditions introduced by polar/spherical coordinate transformation bring some difficulties to theoretical analysis and algorithm implementation. It is significant to propose an effective spectral method for solving the fourth-order problems with complex boundary conditions in some special domains.

Thus, the goal of this paper is to develop a high-order numerical method for fourth-order equation with simply supported plate boundary conditions in a circular domain. By introducing an auxiliary function and using the dimension reduction technique, we reduce the fourth-order problem to a one-dimensional second-order coupled problem. Based on the one-dimensional second-order coupled problem, we prove the uniqueness of the weak solution and approximation solutions and the error estimation between them. Moreover, we extend the approach to fourth-order eigenvalue problem with simply supported plate boundary conditions in a circular domain. Finally, we carry out some numerical experiments to validate the theoretical analysis and algorithm.

The rest of this paper is organized as follows: In Section 2, we reduce the fourth order problem to a coupled second order problem and derive the corresponding dimension reduction scheme. In Section 3, we deduce the weak form and its spectral-Galerkin approximation for the couple second order problem. We give the error estimation of approximation solution in Section 4. An efficient implementation of algorithm is developed in the Section 5. In Section 6, we extend the numerical approaches to eigenvalue problems. In Section 7, some numerical experiments are carried out to validate the results of theoretical analysis and algorithm. Finally we give some concluding remarks.

2. Fourth order problem and its reduced order scheme

As a model, we consider the following fourth-order problem:

$$\Delta^2 \hat{u}(x,y) = \hat{f}(x,y), \quad \text{in } \Omega, \tag{2.1}$$

$$\hat{u}(x,y) = \hat{\varphi}(x,y), \quad \text{on } \partial\Omega, \tag{2.2}$$

$$\Delta \hat{u}(x,y) = \hat{\psi}(x,y), \quad \text{on } \partial\Omega, \tag{2.3}$$

where $\Omega = \{(x,y) : x^2 + y^2 \leq R^2\}$.

We shall transform the original problem (2.1)-(2.3) into a second-order coupled problem. Based on the second-order coupled problem, we further derive the equivalent dimension reduction scheme. We first introduce an auxiliary function:

$$\hat{w}(x,y) = -\Delta \hat{u}(x,y). \tag{2.4}$$

Inserting (2.4) into (2.1) results in:

$$
\begin{aligned}
&-\Delta\hat{w}(x,y)=\hat{f}(x,y), \quad \text{in } \Omega, && (2.5)\\
&-\Delta\hat{u}(x,y)=\hat{w}(x,y), \quad \text{in } \Omega, && (2.6)\\
&\hat{w}(x,y)=-\hat{\psi}(x,y), \qquad \text{on } \partial\Omega, && (2.7)\\
&\hat{u}(x,y)=\hat{\varphi}(x,y), \qquad \text{on } \partial\Omega. && (2.8)
\end{aligned}
$$

Recall the polar coordinate transformation: $x = r\cos\theta$, $y = r\sin\theta$. Let

$$
\begin{aligned}
&u(r,\theta)=\hat{u}(x,y),\ w(r,\theta)=\hat{w}(x,y),\ f(r,\theta)=\hat{f}(x,y),\\
&\varphi(r,\theta)=\hat{\varphi}(x,y),\ \psi(r,\theta)=\hat{\psi}(x,y).
\end{aligned}
$$

Thus the problem (2.5)-(2.8) can be rewritten as the following equivalent form:

$$
\begin{aligned}
&-\frac{1}{r}\frac{\partial}{\partial r}(r\frac{\partial w(r,\theta)}{\partial r})-\frac{1}{r^2}\frac{\partial^2 w(r,\theta)}{\partial\theta^2}=f(r,\theta), \quad (r,\theta)\in D, && (2.9)\\
&-\frac{1}{r}\frac{\partial}{\partial r}(r\frac{\partial u(r,\theta)}{\partial r})-\frac{1}{r^2}\frac{\partial^2 u(r,\theta)}{\partial\theta^2}=w(r,\theta), \quad (r,\theta)\in D, && (2.10)\\
&w(R,\theta)=-\psi(R,\theta), \qquad \theta\in[0,2\pi), && (2.11)\\
&u(R,\theta)=\varphi(R,\theta), \qquad \theta\in[0,2\pi), && (2.12)
\end{aligned}
$$

where $D=[0,R)\times[0,2\pi)$. Without loss of generality, supposing that $\psi(R,\theta) = \varphi(R,\theta) = 0$. We derive from the Fourier expansion of the periodic function that

$$
w(r,\theta)=\sum_{|m|=0}^{\infty}\hat{w}_m(r)e^{im\theta},\ u(r,\theta)=\sum_{|m|=0}^{\infty}\hat{u}_m(r)e^{im\theta},\ f(r,\theta)=\sum_{|m|=0}^{\infty}\hat{f}_m(r)e^{im\theta}. \tag{2.13}
$$

Note that

$$
\begin{aligned}
\Delta\hat{w}(x,y)=\Delta w(r,\theta)&=\frac{\partial^2 w(r,\theta)}{\partial r}+\frac{1}{r}\frac{\partial w(r,\theta)}{\partial r}+\frac{1}{r^2}\frac{\partial^2 w(r,\theta)}{\partial\theta}\\
&=\sum_{|m|=0}^{\infty}[\frac{\partial^2\hat{w}_m(r)}{\partial r}+\frac{1}{r}\frac{\partial\hat{w}_m(r)}{\partial r}-\frac{m^2}{r^2}\hat{w}_m(r)]e^{im\theta}.
\end{aligned} \tag{2.14}
$$

In order to ensure the boundedness of (2.14), we know from [2,3] that the following essential pole conditions should be imposed in order to overcome the singularity introduced by the polar coordinate transformation, i.e.,

$$
m\hat{w}_m|_{r=0}=0,\ m\hat{u}_m|_{r=0}=0,
$$

that is

$$
\hat{w}_m(0)=0,\ \hat{u}_m(0)=0,\ (m\neq 0). \tag{2.15}
$$

Let

$$
r=\frac{t+1}{2}R,\ w_m(t)=\hat{w}_m(r), f_m(t)=\hat{f}_m(r),\ u_m(t)=\hat{u}_m(r).
$$

From (2.13), the pole conditions (2.15) and the orthogonality of Fourier basis functions, (2.9)-(2.12) can be simplified to one-dimensional coupled second order problems:

$$-\frac{1}{t+1}\partial_t((t+1)\partial_t w_m)+\frac{m^2}{(t+1)^2}w_m=\frac{R^2}{4}f_m,\ t\in(-1,1), \tag{2.16}$$

$$-\frac{1}{t+1}\partial_t((t+1)\partial_t u_m)+\frac{m^2}{(t+1)^2}u_m=\frac{R^2}{4}w_m,\ t\in(-1,1), \tag{2.17}$$

$$w_m(1)=u_m(1)=0,\quad (m=0), \tag{2.18}$$

$$w_m(\pm1)=u_m(\pm1)=0,\ (m\neq 0). \tag{2.19}$$

3. Weak form and its spectral-Galerkin approximation

Let $I=(-1,1),\omega=1+t$. Define the usual weighted Sobolev space:

$$L^2_\omega(I):=\Big\{p:\int_I \omega|p|^2dt<\infty\Big\}$$

with the following inner product and norm:

$$(p,q)_\omega=\int_I \omega p\bar{q}dt,\ \|p\|_\omega=[\int_I\omega|p|^2dt]^{\frac{1}{2}}.$$

We further introduce non-uniformly weighted Sobolev spaces $H^1_{0,\omega,m}(I)$:

$$H^1_{0,\omega,m}(I):=\{p_m:\partial_t^k w_m\in L^2_\omega(I),k=1,p_m(1)=0\},\ (m=0);$$
$$H^1_{0,\omega,m}(I):=\{p_m:\partial_t^k w_m\in L^2_{\omega^{2k-1}}(I),k=0,1,p_m(\pm1)=0\},\ (m\neq0),$$

with the following inner products and norms:

$$(p_0,q_0)_{1,\omega,0}:=(\partial_t p_0,\partial_t q_0)_w,\ \|p_0\|_{1,\omega,0}=\sqrt{(p_0,p_0)_{1,\omega,0}};$$
$$(p_m,q_m)_{1,\omega,m}:=\sum_{k=0}^{1}(\partial_t^k p_m,\partial_t^k q_m)_{w^{2k-1}},\ \|p_m\|_{1,\omega,m}=(p_m,p_m)^{\frac{1}{2}}_{1,\omega,m},\ (m\neq0).$$

Then the weak form of (2.16)-(2.19) is : Find $(w_m,u_m)\in H^1_{0,\omega,m}(I)\times H^1_{0,\omega,m}(I)$, such that

$$a_m(w_m,v_m)=F_m(v_m),\qquad \forall v_m\in H^1_{0,\omega,m}(I), \tag{3.1}$$

$$a_m(u_m,h_m)=b_m(w_m,h_m),\ \forall h_m\in H^1_{0,\omega,m}(I), \tag{3.2}$$

where

$$a_m(w_m,v_m)=\int_I(t+1)w_m'v_m'+\frac{m^2}{t+1}w_mv_mdt,$$
$$F_m(v_m)=\frac{R^2}{4}\int_I(t+1)f_mv_mdt,\ b_m(w_m,h_m)=\frac{R^2}{4}\int_I(t+1)w_mh_mdt.$$

Denote by P_N the space of polynomials of degree less than or equal to N. Define an approximation space $X_N(m) = P_N \cap H^1_{0,\omega,m}(I)$. Then the spectral-Galerkin approximation to (3.1)-(3.2) are: Find $(w_{mN}, u_{mN}) \in X_N(m) \times X_N(m)$, such that

$$a_m(w_{mN}, v_{mN}) = F_m(v_{mN}), \qquad \forall v_{mN} \in X_N(m), \tag{3.3}$$

$$a_m(u_{mN}, h_{mN}) = b_m(w_{mN}, h_{mN}), \ \forall h_{mN} \in X_N(m). \tag{3.4}$$

4. Error estimation of approximation solution

Lemma 4.1. *$a_m(w_m, v_m)$ is a continuous and coercive bilinear functional on $H^1_{0,\omega,m}(I) \times H^1_{0,\omega,m}(I)$, i.e.,*

$$|a_m(w_m, v_m)| \le \max\{1, m^2\}\|w_m\|_{1,\omega,m}\|v_m\|_{1,\omega,m},$$
$$a_m(w_m, w_m) \ge \|w_m\|^2_{1,\omega,m}.$$

Proof. When $m = 0$, from Cauchy-Schwarz inequality we have

$$\begin{aligned}
|a_0(w_0, v_0)| &= |\int_I (1+t) w_0'(t) v_0'(t) dt| \\
&\le \int_I (t+1)|w_0'(t)v_0'(t)|dt \\
&\le \left[\int_I (t+1)|w_0'(t)|^2 dt\right]^{\frac{1}{2}} \left[\int_I (t+1)|v_0'(t)|^2 dt\right]^{\frac{1}{2}} \\
&= \|w_0\|_{1,\omega,0}\|v_0\|_{1,\omega,0}, \\
a_0(w_0, w_0) &= \int_I (t+1)|w_0'(t)|^2 dt = \|w_0\|^2_{1,\omega,0}.
\end{aligned}$$

When $m \ne 0$, from Cauchy-Schwarz inequality we derive that

$$\begin{aligned}
|a_m(w_m, v_m)| &= |\int_I ((1+t)w_m'(t)v_m'(t) + \frac{m^2}{t+1} w_m(t)v_m(t))dt| \\
&\le m^2 \int_I ((t+1)|w_m'(t)v_m'(t)| + \frac{1}{t+1}|w_m(t)v_m(t)|)dt \\
&\le m^2 \left[\int_I ((t+1)|w_m'(t)|^2 + \frac{1}{t+1}|w_m(t)|^2)dt\right]^{\frac{1}{2}}, \\
&\quad \left[\int_I ((t+1)|v_m'(t)|^2 + \frac{1}{t+1}|v_m(t)|^2)dt\right]^{\frac{1}{2}} \\
&= m^2 \|w_m\|_{1,\omega,m}\|v_m\|_{1,\omega,m}, \\
a_m(w_m, w_m) &= \int_I ((t+1)|w_m'(t)|^2 + \frac{m^2}{1+t}|w_m(t)|^2)dt \\
&\ge \int_I ((t+1)|w_m'|^2 + \frac{1}{1+t}|w_m|^2)dt = \|w_m\|^2_{1,\omega,m}.
\end{aligned}$$

This finishes our proof. □

Lemma 4.2. *For $\forall w_m \in H^1_{0,\omega,m}(I)$, the following inequality holds:*

$$\int_I (t+1) w_m^2(t) dt \le \int_I (t+1)[w_m'(t)]^2 dt.$$

Proof. It follows from the boundary condition $w(1) = 0$ that

$$-w_m(t) = \int_t^1 w_m'(s)ds. \tag{4.1}$$

From Cauchy-Schwarz inequality and (4.1), we derive that

$$\begin{aligned}
\int_{-1}^1 (t+1)w_m^2(t)dt &= \int_{-1}^1 \left[\int_t^1 \frac{1}{\sqrt{s+1}}\sqrt{s+1}w_m'(s)ds\right]^2 (t+1)dt \\
&\leq \int_{-1}^1 \int_t^1 (s+1)[w_m'(s)]^2 ds[\ln 2 - \ln(t+1)](t+1)dt \\
&\leq \int_{-1}^1 (s+1)[w_m'(s)]^2 ds \int_{-1}^1 [(t+1)\ln 2 - (t+1)\ln(t+1)]dt \\
&= \int_{-1}^1 (s+1)[w_m'(s)]^2 ds = \int_{-1}^1 (t+1)[w_m'(t)]^2 dt.
\end{aligned}$$

This finishes our proof. □

Lemma 4.3. *If $f_m(t) \in L^2_\omega(I)$, then $F_m(v_m)$ is a bounded linear functional on $H^1_{0,\omega,m}(I)$, i.e.,*

$$|F_m(v_m)| \lesssim \|v_m\|_{1,\omega,m}.$$

Proof. From the Cauchy-Schwarz inequality and Lemma 4.2, we have

$$\begin{aligned}
|F_m(v_m)| &= |\int_I (t+1)f_m(t)v_m(t)dt| \\
&\leq \left[\int_I (t+1)|f_m(t)|^2 dt\right]^{\frac{1}{2}} \left[\int_I (t+1)|v_m(t)|^2 dt\right]^{\frac{1}{2}} \\
&\lesssim (\int_I (t+1)|v_m(t)|^2 dt)^{\frac{1}{2}} \\
&\lesssim (\int_I (t+1)|v_m'|^2 dt)^{\frac{1}{2}} \\
&= \|v_m\|_{1,\omega,m}.
\end{aligned}$$

This finishes our proof. □

From Lemma 4.1, Lemma 4.3 and Lax-Milgram Lemma, we have following Theorem:

Theorem 4.1. *If $f_m(t) \in L^2_\omega(I)$, then problems* (3.1)-(3.2) *and* (3.3)-(3.4) *have unique solutions $(w_m, u_m) \in H^1_{0,\omega,m} \times H^1_{0,\omega,m}$ and $(w_{mN}, u_{mN}) \in X_N(m) \times X_N(m)$, respectively.*

Lemma 4.4. *Assuming that w_m and w_{mN} are the solutions of* (3.1) *and* (3.3), *respectively, there holds:*

$$\|w_m - w_{mN}\|_{1,\omega,m} \leq \max\{\sqrt{2}, 4m^3\} \inf_{v_{mN} \in X_N(m)} \|\partial_t(w_m - v_{mN})\|.$$

Proof. From (3.1) and (3.3), we have

$$a_m(w_m, v_{mN}) = F_m(v_{mN}),\ \forall v_{mN} \in X_N(m), \tag{4.2}$$

$$a_m(w_{mN}, v_{mN}) = F_m(v_{mN}),\ \forall v_{mN} \in X_N(m), \tag{4.3}$$

which leads to

$$a_m(w_m - w_{mN}, v_{mN}) = 0,\ \forall v_{mN} \in X_N(m). \tag{4.4}$$

When $m = 0$, one can deduce form Lemma 4.1 and (4.4) that

$$\begin{aligned}
&\|w_m - w_{mN}\|^2_{1,\omega,m} \\
\leq & a_m(w_m - w_{mN}, w_m - w_{mN}) \\
= & a_m(w_m - w_{mN}, w_m - v_{mN} + v_{mN} - w_{mN}) \\
= & a_m(w_m - w_{mN}, w_m - v_{mN}) + a_m(w_m - w_{mN}, v_{mN} - w_{mN}) \\
\leq & \|w_m - w_{mN}\|_{1,\omega,m} \|w_m - v_{mN}\|_{1,\omega,m},
\end{aligned}$$

this implies that

$$\|w_m - w_{mN}\|_{1,\omega,m} \leq \|w_m - v_{mN}\|_{1,\omega,m},\ \forall v_{mN} \in X_N(m).$$

Since

$$\|w_m - v_{mN}\|^2_{1,\omega,m} = \int_I (t+1)[\partial_t(w_m - v_{mN})]^2 dt \leq 2\|\partial_t(w_m - v_{mN})\|^2,$$

it is easy to show that

$$\|w_m - w_{mN}\|_{1,\omega,m} \leq \sqrt{2}\|\partial_t(w_m - v_{mN})\|. \tag{4.5}$$

When $m \neq 0$, we obtain from Lemma 4.1 and (4.4) that

$$\begin{aligned}
&\|w_m - w_{mN}\|^2_{1,\omega,m} \\
\leq & a_m(w_m - w_{mN}, w_m - w_{mN}) \\
= & a_m(w_m - w_{mN}, w_m - v_{mN} + v_{mN} - w_{mN}) \\
= & a_m(w_m - w_{mN}, w_m - v_{mN}) + a_m(w_m - w_{mN}, v_{mN} - w_{mN}) \\
\leq & m^2\|w_m - w_{mN}\|_{1,\omega,m} \|w_m - v_{mN}\|_{1,\omega,m},
\end{aligned}$$

that is

$$\|w_m - w_{mN}\|_{1,\omega,m} \leq m^2\|w_m - v_{mN}\|_{1,\omega,m},\ \forall v_{mN} \in X_N(m).$$

Using the pole condition $w_m(-1) = 0$ and Hardy inequality (cf. B8.6 in [21]), we obtain that

$$\int_I \frac{1}{(1+t)^2} w_m^2 dt \leq 4\int_I (\partial_t w_m)^2 dt.$$

We then have

$$\begin{aligned}
\|w_m - v_{mN}\|^2_{1,\omega,m} &= \int_I (t+1)[\partial_t(w_m - v_{mN})]^2 dt + \int_I \frac{m^2}{t+1}(w_m - v_{mN})^2 dt \\
&\leq \int_I (t+1)[\partial_t(w_m - v_{mN})]^2 dt + 2m^2 \int_I \frac{1}{(t+1)^2}(w_m - v_{mN})^2 dt
\end{aligned}$$

$$\leq \int_I (t+1)[\partial_t(w_m - v_{mN})]^2 dt + 8m^2 \int_I [\partial_t(w_m - v_{mN})]^2 dt$$
$$\leq 16m^2 \int_I [\partial_t(w_m - v_{mN})]^2 dt.$$

Thus

$$\|w_m - w_{mN}\|_{1,\omega,m} \leq 4m^3 \left[\int_I (\partial_t(w_m - v_{mN}))^2 dt \right]^{\frac{1}{2}} = 4m^3 \|\partial_t(w_m - v_{mN})\|. \tag{4.6}$$

The expected result follows from inequalities (4.5), (4.6) and the arbitrariness of v_{mN}. This finishes our proof. $\square$

For proving the error estimation, we need to introduce two non-uniformly weighted Sobolev spaces as follows:

$$H^s_{\omega^{\alpha,\beta},*}(I) := \{w : \partial_t^k w \in L^2_{\omega^{\alpha+k,\beta+k}}, 0 \leq k \leq s\},$$

equipped with the inner product and the associated norm

$$(w,v)_{s,\omega^{\alpha,\beta},*} = \sum_{k=0}^{s} (\partial_t^k w, \partial_t^k v)_{\omega^{\alpha+k,\beta+k}},\ \|w\|_{s,\omega^{\alpha,\beta},*} = \sqrt{(w,w)_{s,\omega^{\alpha,\beta},*}}$$

and

$$\hat{\mathcal{H}}^s_{\omega^{-1,-1},m}(I) := \{w_m \in H^1_{0,\omega,m}(I) : \partial_t^k w_m \in L^2_{\omega^{-1+k,-1+k}},\ 1 \leq k \leq s\},$$

equipped with the inner product and the associated norm

$$(w_m, v_m)_{s,\omega^{-1,-1},m} = (w_m, v_m)_{1,\omega,m} + \sum_{k=1}^{s} (\partial_t^k w_m, \partial_t^k v_m)_{\omega^{-1+k,-1+k}},$$
$$\|w_m\|_{s,\omega^{-1,-1},m} = \sqrt{(w_m, w_m)_{s,\omega^{-1,-1},m}},$$

where $\omega^{\alpha,\beta}(t) = (1-t)^\alpha(1+t)^\beta$ is Jacobi weight function.

Define an orthogonal projection operator $\Pi_{N,\omega^{-1,-1}} : L^2_{\omega^{-1,-1}}(I) \to P_N^{-1,-1}$ such that

$$(w - \Pi_{N,\omega^{-1,-1}} w, v_N)_{\omega^{-1,-1}} = 0,\ \forall v_N \in P_N^{-1,-1}, \tag{4.7}$$

where $P_N^{-1,-1} = \{p \in P_N : p(\pm 1) = 0\}$.

From Theorem 1.8.2 in [20] we have following Lemma:

Lemma 4.5. *For $\forall w \in H^s_{\omega^{-1,-1},*}(I)$, the following inequality holds:*

$$\|\partial_t(\Pi_{N,\omega^{-1,-1}} w - w)\| \lesssim N^{1-s} \|\partial_t^s w\|_{\omega^{-1+s,-1+s}}.$$

Theorem 4.2. *There exist an operator $\Pi_N^{1,0} : H^1_{0,\omega,0}(I) \to P_N^0$ such that $\Pi_N^{1,0} w_0(-1) = w_0(-1)$, $\Pi_N^{1,0} w_0(1) = w_0(1) = 0$, for any $w_0 \in \hat{\mathcal{H}}^s_{\omega^{-1,-1},0}(I)$ $(s \geq 1)$, there holds*

$$\|\partial_t(\Pi_N^{1,0} w_0 - w_0)\| \lesssim N^{1-s} \|\partial_t^s w_0\|_{\omega^{-1+s,-1+s}},$$

where $P_N^0 = \{p_0 \in P_N : p_0(1) = 0\}$.

Proof. Let $w_0^*(t)=\frac{1-t}{2}w_0(-1)$, $\forall w_0\in H^1_{0,\omega,0}(I)$. Then for $\forall w_0\in\hat{\mathcal{H}}^s_{\omega^{-1,-1},0}(I)$, we have $(w_0-w_0^*)(\pm1)=0$, and $w_0-w_0^*\in H^s_{\omega^{-1,-1},*}(I)$. In fact, we derive from Hardy inequality (cf. B8.8 in [21]) that

$$\int_I\omega^{-1,-1}(w_0-w_0^*)^2dt\lesssim\int_I\omega^{-2,-2}(w_0-w_0^*)^2dt\lesssim\int_I[\partial_t(w_0-w_0^*)]^2dt.$$

Since

$$\begin{aligned}\int_I[\partial_t w_0^*]^2dt&=\int_I\frac{1}{4}[w_0(-1)]^2dt=\frac{1}{2}[w_0(-1)]^2\\&=\frac{1}{2}\Big[\int_I(\partial_t w_0)dt\Big]^2\lesssim\int_I(\partial_t w_0)^2dt,\end{aligned}$$

we then obtain

$$\int_I[\partial_t(w_0-w_0^*)]^2dt\lesssim\int_I(\partial_t w_0)^2dt+\int_I(\partial_t w_0^*)^2dt\lesssim\int_I(\partial_t w_0)^2dt. \tag{4.8}$$

For $k\geqslant 2$, we have

$$\int_I\omega^{-1+k,-1+k}[\partial_t^k(w_0-w_0^*)]^2dt\lesssim\int_I\omega^{-1+k,-1+k}(\partial_t^k w_0)^2dt. \tag{4.9}$$

Thus $w_0-w_0^*\in H^s_{\omega^{-1,-1},*}(I)$. Define

$$\Pi_N^{1,0}w_0=\Pi_{N,\omega^{-1,-1}}(w_0-w_0^*)+w_0^*\in P_N^0,\ \forall w_0\in\mathcal{H}^s_{\omega^{-1,-1},0}(I).$$

In light of Lemma 4.5 we have

$$\begin{aligned}\|\partial_t(\Pi_N^{1,0}w_0-w_0)\|&=\|\partial_t[\Pi_{N,\omega^{-1,-1}}(w_0-w_0^*)-(w_0-w_0^*)]\|\\&\lesssim N^{1-s}\|\partial_t^s(w_0-w_0^*)\|_{\omega^{-1+s,-1+s}}\\&\lesssim N^{1-s}\|\partial_t^s w_0\|_{\omega^{-1+s,-1+s}}.\end{aligned}$$

This finishes our proof. □

Theorem 4.3. *Let w_m and w_{mN} be the solutions of* (3.1) *and* (3.3), *respectively. If $m=0$, and $w_m\in\hat{\mathcal{H}}^s_{\omega^{-1,-1},m}(I)(s\geq1)$, then the following inequality holds*

$$\|w_m-w_{mN}\|_{1,\omega,m}\lesssim N^{1-s}\|\partial_t^s w_m\|_{\omega^{-1+s,-1+s}}.$$

If $m\neq0$ and $w_m\in H^1_{0,\omega,m}(I)\cap H^s_{\omega^{-1,-1},*}(I)(s\geq1)$, then the following inequality holds

$$\|w_m-w_{mN}\|_{1,\omega,m}\lesssim N^{1-s}\|\partial_t^s w_m\|_{\omega^{-1+s,-1+s}}.$$

Proof. When $m=0$, for $\forall v_{0N}\in X_N(0)$, from Lemma 4.4 and Theorem 4.2 we have

$$\begin{aligned}\|w_0-w_{0N}\|_{1,\omega,0}&\leq\inf_{v_{0N}\in X_N(0)}\sqrt{2}\|\partial_t(w_0-v_{0N})\|\\&\lesssim\|\partial_t(w_0-\Pi_N^{1,0}w_0)\|\\&\lesssim N^{1-s}\|\partial_t^s w_0\|_{\omega^{-1+s,-1+s}}.\end{aligned}$$

When $m \neq 0$, for $\forall v_{mN} \in X_N(m)$, from Lemma 4.4 and Lemma 4.5 we arrive at

$$\begin{aligned}\|w_m - w_{mN}\|_{1,\omega,m} \leq & \inf_{v_{mN}\in X_N(m)} 4m^3\|\partial_t(w_m - v_{mN})\| \\ & \lesssim \|\partial_t(w_m - \Pi_{N,\omega^{-1,-1}} w_m)\| \lesssim N^{1-s}\|\partial_t^s w_m\|_{\omega^{-1+s,-1+s}}.\end{aligned}$$

This finishes our proof. □

Theorem 4.4. *Let u_m and u_{mN} be the solutions of* (3.2) *and* (3.4)*, respectively. Then the following inequality holds*

$$\|u_m - u_{mN}\|_{1,\omega,m} \lesssim N^{1-s}\big[\|\partial_t^s u_m\|_{\omega^{-1+s,-1+s}} + \|\partial_t^s w_m\|_{\omega^{-1+s,-1+s}}\big].$$

Proof. From(3.2) and (3.4) we have

$$a_m(u_m, h_{mN}) = b_m(w_m, h_{mN}),\ \forall\ h_{mN} \in X_N(m), \tag{4.10}$$
$$a_m(u_{mN}, h_{mN}) = b_m(w_{mN}, h_{mN}),\ \forall\ h_{mN} \in X_N(m), \tag{4.11}$$

which leads to

$$a_m(u_m - u_{mN}, h_{mN}) = b_m(w_m - w_{mN}, h_{mN}),\ \forall h_{mN} \in X_N(m). \tag{4.12}$$

When $m = 0$, for $\forall q_{mN} \in X_N(m)$, we obtain from Lemma 4.1, Lemma 4.2 and (4.12) that

$$\begin{aligned}&\|u_m - u_{mN}\|^2_{1,\omega,m}\\ \leq & a_m(u_m - u_{mN}, u_m - u_{mN})\\ = & a_m(u_m - u_{mN}, u_m - q_{mN} + q_{mN} - u_{mN})\\ = & a_m(u_m - u_{mN}, u_m - q_{mN}) + a_m(u_m - u_{mN}, q_{mN} - u_{mN})\\ = & a_m(u_m - u_{mN}, u_m - q_{mN}) + b_m(w_m - w_{mN}, q_{mN} - u_{mN})\\ \leq & \|u_m - u_{mN}\|_{1,\omega,m}\|u_m - q_{mN}\|_{1,\omega,m}\\ & + \frac{R^2}{4}\|w_m - w_{mN}\|_{1,\omega,m}\|q_{mN} - u_{mN}\|_{1,\omega,m}.\end{aligned}$$

By taking $q_{mN} = \Pi_N^{1,0} u_m$, we obtain

$$\begin{aligned}\|u_m - u_{mN}\|^2_{1,\omega,m} \leq & \|u_m - u_{mN}\|_{1,\omega,m}\|u_m - \Pi_N^{1,0}u_m\|_{1,\omega,m}\\ & + \frac{R^2}{4}\|w_m - w_{mN}\|_{1,\omega,m}\|\Pi_N^{1,0}u_m - u_{mN}\|_{1,\omega,m}.\end{aligned}$$

Since

$$\begin{aligned}\|\Pi_N^{1,0}u_m - u_{mN}\|_{1,\omega,m} &= \|\Pi_N^{1,0}u_m - u_m + u_m - u_{mN}\|_{1,\omega,m}\\ &\leq \|\Pi_N^{1,0}u_m - u_m\|_{1,\omega,m} + \|u_m - u_{mN}\|_{1,\omega,m},\end{aligned}$$

then

$$\begin{aligned}&\|u_m - u_{mN}\|^2_{1,\omega,m}\\ \leq & \|u_m - u_{mN}\|_{1,\omega,m}\|u_m - \Pi_N^{1,0}u_m\|_{1,\omega,m}\\ & + \frac{R^2}{4}\|w_m - w_{mN}\|_{1,\omega,m}\|\Pi_N^{1,0}u_m - u_m\|_{1,\omega,m}\end{aligned}$$

$$
\begin{aligned}
&+\frac{R^2}{4}\|w_m-w_{mN}\|_{1,\omega,m}\|u_m-u_{mN}\|_{1,\omega,m}\\
\le&\frac{1}{4}\|u_m-u_{mN}\|^2_{1,\omega,m}+\|u_m-\Pi_N^{1,0}u_m\|^2_{1,\omega,m}+\frac{R^4}{32}\|w_m-w_{mN}\|^2_{1,\omega,m}\\
&+\frac{1}{2}\|\Pi_N^{1,0}u_m-u_m\|^2_{1,\omega,m}+\frac{R^4}{16}\|w_m-w_{mN}\|^2_{1,\omega,m}+\frac{1}{4}\|u_m-u_{mN}\|^2_{1,\omega,m}.
\end{aligned}
$$

One can derive from above inequality that

$$
\|u_m-u_{mN}\|^2_{1,\omega,m}\le 3[\|u_m-\Pi_N^{1,0}u_m\|^2_{1,\omega,m}+\frac{R^4}{16}\|w_m-w_{mN}\|^2_{1,\omega,m}].
$$

From Theorem 4.2 and Theorem 4.3, we have

$$
\begin{aligned}
\|u_m-u_{mN}\|^2_{1,\omega,m}&\lesssim[N^{1-s}\|\partial_t^s u_m\|_{\omega^{-1+s,-1+s}}]^2+[N^{1-s}\|\partial_t^s w_m\|_{\omega^{-1+s,-1+s}}]^2\\
&\le[N^{1-s}\|\partial_t^s u_m\|_{\omega^{-1+s,-1+s}}+N^{1-s}\|\partial_t^s w_m\|_{\omega^{-1+s,-1+s}}]^2,
\end{aligned}
$$

that is

$$
\|u_m-u_{mN}\|_{1,\omega,m}\lesssim N^{1-s}(\|\partial_t^s u_m\|_{\omega^{-1+s,-1+s}}+\|\partial_t^s w_m\|_{\omega^{-1+s,-1+s}}). \tag{4.13}
$$

When $m\neq 0$, for $\forall q_{mN}\in X_N(m)$, in accordance with Lemma 4.1, Lemma 4.2 and (4.12) we obatin

$$
\begin{aligned}
&\|u_m-u_{mN}\|^2_{1,\omega,m}\\
\le&a_m(u_m-u_{mN},u_m-u_{mN})\\
=&a_m(u_m-u_{mN},u_m-q_{mN}+q_{mN}-u_{mN})\\
=&a_m(u_m-u_{mN},u_m-q_{mN})+a_m(u_m-u_{mN},q_{mN}-u_{mN})\\
=&a_m(u_m-u_{mN},u_m-q_{mN})+b_m(w_m-w_{mN},q_{mN}-u_{mN})\\
\le&m^2\|u_m-u_{mN}\|_{1,\omega,m}\|u_m-q_{mN}\|_{1,\omega,m}\\
&+\frac{R^2}{4}\|w_m-w_{mN}\|_{1,\omega,m}\|q_{mN}-u_{mN}\|_{1,\omega,m}.
\end{aligned}
$$

By $q_{mN}=\Pi_{N,\omega^{-1,-1}}u_m$, we have

$$
\begin{aligned}
\|u_m-u_{mN}\|^2_{1,\omega,m}\le&m^2\|u_m-u_{mN}\|_{1,\omega,m}\|u_m-\Pi_{N,\omega^{-1,-1}}u_m\|_{1,\omega,m}\\
&+\frac{R^2}{4}\|w_m-w_{mN}\|_{1,\omega,m}\|\Pi_{N,\omega^{-1,-1}}u_m-u_{mN}\|_{1,\omega,m}.
\end{aligned}
$$

Since

$$
\begin{aligned}
\|\Pi_{N,\omega^{-1,-1}}u_m-u_{mN}\|_{1,\omega,m}&=\|\Pi_{N,\omega^{-1,-1}}u_m-u_m+u_m-u_{mN}\|_{1,\omega,m}\\
&\le\|\Pi_{N,\omega^{-1,-1}}u_m-u_m\|_{1,\omega,m}+\|u_m-u_{mN}\|_{1,\omega,m},
\end{aligned}
$$

then

$$
\begin{aligned}
\|u_m-u_{mN}\|^2_{1,\omega,m}\le&m^2\|u_m-u_{mN}\|_{1,\omega,m}\|u_m-\Pi_{N,\omega^{-1,-1}}u_m\|_{1,\omega,m}\\
&+\frac{R^2}{4}\|w_m-w_{mN}\|_{1,\omega,m}\|\Pi_{N,\omega^{-1,-1}}u_m-u_m\|_{1,\omega,m}\\
&+\frac{R^2}{4}\|w_m-w_{mN}\|_{1,\omega,m}\|u_m-u_{mN}\|_{1,\omega,m}
\end{aligned}
$$

$$
\begin{aligned}
&\le \frac{1}{4}\|u_m - u_{mN}\|^2_{1,\omega,m} + m^4\|u_m - \Pi_{N,\omega^{-1,-1}}u_m\|^2_{1,\omega,m}\\
&\quad + \frac{R^4}{32}\|w_m - w_{mN}\|^2_{1,\omega,m} + \frac{1}{2}\|\Pi_{N,\omega^{-1,-1}}u_m - u_m\|^2_{1,\omega,m}\\
&\quad + \frac{R^4}{16}\|w_m - w_{mN}\|^2_{1,\omega,m} + \frac{1}{4}\|u_m - u_{mN}\|^2_{1,\omega,m},
\end{aligned}
$$

that is

$$
\|u_m - u_{mN}\|^2_{1,\omega,m} \le (2m^4+1)\|u_m - \Pi_{N,\omega^{-1,-1}}u_m\|^2_{1,\omega,m} + \frac{3R^4}{16}\|w_m - w_{mN}\|^2_{1,\omega,m}.
$$

According to Lemma 4.5 and Theorem 4.3 we arrive at

$$
\begin{aligned}
\|u_m - u_{mN}\|^2_{1,\omega,m} &\lesssim [N^{1-s}\|\partial_t^s u_m\|_{\omega^{-1+s,-1+s}}]^2 + [N^{1-s}\|\partial_t^s w_m\|_{\omega^{-1+s,-1+s}}]^2\\
&\lesssim [N^{1-s}\|\partial_t^s u_m\|_{\omega^{-1+s,-1+s}} + N^{1-s}\|\partial_t^s w_m\|_{\omega^{-1+s,-1+s}}]^2.
\end{aligned}
$$

Thus

$$
\|u_m - u_{mN}\|_{1,\omega,m} \lesssim N^{1-s}(\|\partial_t^s u_m\|_{\omega^{-1+s,-1+s}} + \|\partial_t^s w_m\|_{\omega^{-1+s,-1+s}}). \tag{4.14}
$$

The desirable result follows from (4.13) and (4.14). This finishes our proof. □

5. Efficient implementation of algorithm

We shall develop an efficient numerical method to solve (3.3)-(3.4). Let us first construct a set of basis functions for the approximation space $X_N(m)$. Let

$$
\phi_i(t) = L_i(t) - L_{i+2}(t),\ i = 0,\cdots,N-2, \tag{5.1}
$$

where $L_i(t)$ represents the Legendre polynomial with degree of i. It is obvious that

$$
\begin{aligned}
&X_N(0) = \mathrm{span}\{\phi_0(t),\cdots,\ \phi_{N-2}(t)\} \oplus \mathrm{span}\{\phi_{N-1}(t)\},\\
&X_N(m) = \mathrm{span}\{\phi_0(t),\cdots,\ \phi_{N-2}(t)\},\ (m \ne 0),
\end{aligned}
$$

where $\phi_{N-1}(t) = \frac{1}{2}(1-t)$. Setting

$$
\begin{aligned}
a_{ij} &= \int_I (t+1)\phi_i'\phi_j' dt,\ b_{ij} = \int_I \frac{1}{1+t}\phi_i\phi_j dt,\\
c_{ij} &= \int_I (t+1)\phi_i\phi_j dt,\ f_i^m = \int_I (t+1) f_m\phi_i dt.
\end{aligned}
$$

When $m = 0$, we shall seek

$$
w_{0N} = \sum_{i=0}^{N-1} w_i^0\phi_i(t),\ u_{0N} = \sum_{i=0}^{N-1} u_i^0\phi_i(t). \tag{5.2}
$$

Plugging (5.2) into (3.3)-(3.4) and taking v_{0N}, h_{0N} through all the basis functions in $X_N(0)$, we derive that

$$
\begin{bmatrix} A_0 & \mathbf{0} \\ -\frac{R^2}{4}C_0 & A_0 \end{bmatrix}\begin{bmatrix} W^0 \\ U^0 \end{bmatrix} = \begin{bmatrix} \frac{R^2}{4}F^0 \\ \mathbf{0} \end{bmatrix},
$$

where

$$A_0 = (a_{ij}),\ C_0 = (c_{ij}),\ F^0 = (f_0^0, \cdots, f_{N-1}^0)^T,$$
$$W^0 = (w_0^0, \cdots, w_{N-1}^0)^T,\ U^0 = (u_0^0, \cdots, u_{N-1}^0)^T.$$

When $m \neq 0$, we shall seek

$$w_{mN} = \sum_{i=0}^{N-2} w_i^m \phi_i(t),\ u_{mN} = \sum_{i=0}^{N-2} u_i^m \phi_i(t). \tag{5.3}$$

Similarly, plugging (5.3) into (3.3)-(3.4) and taking v_{mN}, h_{mN} through all the basis functions in $X_N(m)$, we derive that

$$\begin{bmatrix} A_m + m^2 B_m & \mathbf{0} \\ -\frac{R^2}{4} C_m & A_m + m^2 B_m \end{bmatrix} \begin{bmatrix} W^m \\ U^m \end{bmatrix} = \begin{bmatrix} \frac{R^2}{4} F^m \\ \mathbf{0} \end{bmatrix},$$

where

$$A_m = (a_{ij}),\ B_m = (b_{ij}),\ C_m = (c_{ij}),\ F^m = (f_0^m, \cdots, f_{N-2}^m)^T,$$
$$W^m = (w_0^m, \cdots, w_{N-2}^m)^T,\ U^m = (u_0^m, \cdots, u_{N-2}^m)^T.$$

6. Extension to eigenvalue problems

In this section, we shall extend our algorithm to the associated eigenvalue problems:

$$\Delta^2 \hat{u}(x,y) - \alpha \Delta \hat{u}(x,y) + \beta \hat{u}(x,y) = \lambda \hat{u}(x,y),\ \text{in } \Omega, \tag{6.1}$$
$$\hat{u}(x,y) = 0, \quad \text{on } \partial\Omega, \tag{6.2}$$
$$\Delta \hat{u}(x,y) = 0,\ \text{on } \partial\Omega, \tag{6.3}$$

where α and β are nonnegative constants. Similar to the deduction of (2.16)-(2.19), (6.1)-(6.3) can be reduced to one-dimensional coupled second order eigenvalue problems:

$$-\mathcal{L}_m w_m + \alpha \frac{R^2}{4} w_m + \beta \frac{R^2}{4} u_m = \frac{R^2}{4} \lambda_m u_m, t \in (-1,1), \tag{6.4}$$
$$-\mathcal{L}_m u_m - \frac{R^2}{4} w_m = 0, t \in (-1,1), \tag{6.5}$$
$$u_m(1) = w_m(1) = 0, (m = 0); \tag{6.6}$$
$$u_m(\pm 1) = w_m(\pm 1) = 0, (m \neq 0), \tag{6.7}$$

where

$$\mathcal{L}_m = \frac{1}{t+1} \partial_t((t+1)\partial_t) - \frac{m^2}{(t+1)^2}.$$

Obviously the weak form of (6.4)-(6.7) is: Find $\lambda_m \in \mathbb{R}$, non-trivial $(w_m, u_m) \in H^1_{0,\omega,m}(I) \times H^1_{0,\omega,m}(I)$ such that

$$a_m(w_m, v_m) + \alpha b_m(w_m, v_m) + \beta b_m(u_m, v_m) = \lambda_m b_m(u_m, v_m),\ \forall v_m \in H^1_{0,\omega,m}(I), \tag{6.8}$$

$$a_m(u_m, h_m) - b_m(w_m, h_m) = 0, \ \forall h_m \in H^1_{0,\omega,m}(I). \tag{6.9}$$

Then the spectral-Galerkin approximation to (6.8)-(6.9) is: Find $\lambda_{mN} \in \mathbb{R}$, nontrivial $(w_{mN}, u_{mN}) \in X_N(m) \times X_N(m)$ such that for $\forall (v_{mN}, h_{mN}) \in X_N(m) \times X_N(m)$,

$$a_m(w_{mN}, v_{mN}) + \alpha b_m(w_{mN}, v_{mN}) + \beta b_m(u_{mN}, v_{mN}) = \lambda_{mN} b_m(u_{mN}, v_{mN}), \tag{6.10}$$

$$a_m(u_{mN}, h_{mN}) - b_m(w_{mN}, h_{mN}) = 0. \tag{6.11}$$

When $m = 0$, we shall seek

$$w_{0N} = \sum_{i=0}^{N-1} w_i^0 \phi_i(t), \ u_{0N} = \sum_{i=0}^{N-1} u_i^0 \phi_i(t). \tag{6.12}$$

Plugging (6.12) into (6.10)-(6.11) and taking v_{0N}, h_{0N} through all the basis functions in $X_N(0)$, we derive that

$$\begin{bmatrix} A_0 + \frac{R^2}{4}\alpha C_0 & \frac{R^2}{4}\beta C_0 \\ -\frac{R^2}{4} C_0 & A_0 \end{bmatrix} \begin{bmatrix} W^0 \\ U^0 \end{bmatrix} = \lambda_{0N} \begin{bmatrix} \mathbf{0} & \frac{R^2}{4} C_0 \\ \mathbf{0} & \mathbf{0} \end{bmatrix} \begin{bmatrix} W^0 \\ U^0 \end{bmatrix}.$$

When $m \neq 0$, we shall seek

$$w_{mN} = \sum_{i=0}^{N-2} w_i^m \phi_i(t), \ u_{mN} = \sum_{i=0}^{N-2} u_i^m \phi_i(t). \tag{6.13}$$

Similarly, plugging (6.13) into (6.10)-(6.11) and taking v_{mN}, h_{mN} through all the basis functions in $X_N(m)$, we derive that

$$\begin{bmatrix} A_m + m^2 B_m + \frac{R^2}{4}\alpha C_m & \frac{R^2}{4}\beta C_m \\ -\frac{R^2}{4} C_m & A_m + m^2 B_m \end{bmatrix} \begin{bmatrix} W^m \\ U^m \end{bmatrix} = \lambda_{mN} \begin{bmatrix} \mathbf{0} & \frac{R^2}{4} C_m \\ \mathbf{0} & \mathbf{0} \end{bmatrix} \begin{bmatrix} W^m \\ U^m \end{bmatrix}.$$

Remark 6.1. For the analysis of convergence of the approximating eigenvalues and eigenfunctions in the discrete scheme (6.10)-(6.11), by employing Babuška-Osborn theory, we can establish the abstract spectral approximation results, which combine the approximation properties of projection operators in Section 4 to further obtain the error estimates for approximating eigenvalues and eigenfunctions. For the sake of brevity, we omitted the details.

7. Numerical experiments

We shall present in this section a sequence of numerical experiments to illustrate the effectiveness and high accuracy of our algorithm. We operate our programs in MATLAB 2019b.

Denote by $(\hat{w}_{MN}, \hat{u}_{MN})$ the approximation solutions of the exact solutions $(\hat{w}(x,y), \hat{u}(x,y))$, respectively. According to the pole coordinate transformation and variable substitution we have

$$(\hat{w}(x,y), \hat{u}(x,y)) = (w(t,\theta), u(t,\theta)) = \sum_{|m|=0}^{\infty} (w_m(t), u_m(t)) e^{im\theta},$$

Table 1. The error $e(\hat{w}(x,y), \hat{w}_{MN}(x,y))$ between approximate solutions and exact solutions for different M and different N.

N	$M=4$	$M=8$	$M=12$	$M=16$
20	0.0071	3.6115e-07	3.0101e-06	0.0212
25	0.0072	3.5027e-07	7.1085e-12	1.6536e-07
30	0.0073	3.6103e-07	3.7357e-12	1.4921e-13
35	0.0073	3.5619e-07	2.3093e-14	2.0359e-16

$$(\hat{w}_{MN}(x,y), \hat{u}_{MN}(x,y)) = (w_{MN}(t,\theta), u_{MN}(t,\theta)) = \sum_{|m|=0}^{M} (w_{mN}(t), u_{mN}(t))e^{im\theta}.$$

Define the errors between the weak solutions $(\hat{w}(x,y), \hat{u}(x,y))$ and the numerical solutions $(\hat{w}_{MN}, \hat{u}_{MN})$ as follows:

$$\begin{aligned} e(\hat{w}(x,y), \hat{w}_{MN}(x,y)) &= \|\hat{w}(x,y) - \hat{w}_{MN}(x,y)\|_{L^\infty(\Omega)} \\ &= \|w(t,\theta) - w_{MN}(t,\theta)\|_{L^\infty(D)}, \end{aligned}$$

and

$$\begin{aligned} e(\hat{u}(x,y), \hat{u}_{MN}(x,y)) &= \|\hat{u}(x,y) - \hat{u}_{MN}(x,y)\|_{L^\infty(\Omega)} \\ &= \|u(t,\theta) - u_{MN}(t,\theta)\|_{L^\infty(D)}. \end{aligned}$$

Example 7.1. We take $R = 1$, $\hat{u} = (x^2 + y^2 - 1)^3 e^{x+y}$. By plugging $\hat{u}(x,y)$ into equations (2.1)-(2.3), we can obtain $\hat{f}(x,y), \hat{\varphi}(x,y)$ and $\hat{\psi}(x,y)$. For different N and M, the errors between approximate solutions and exact solutions are listed in Tables 1-2. To further demonstrate the efficiency and accuracy of our algorithm, we draw the images of the exact solutions and the approximate solutions in Figures 1 and 3 and the error images between them in Figures 2 and 4.

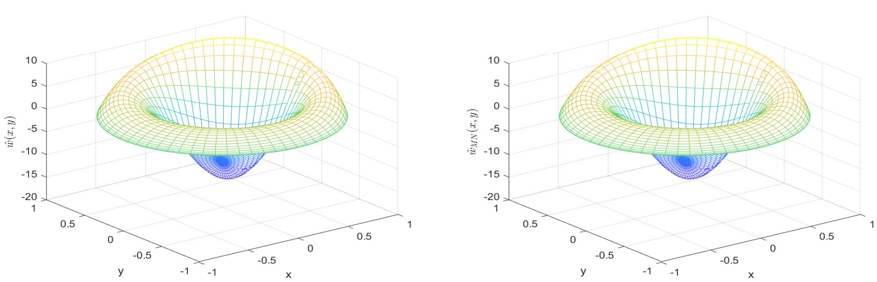

Figure 1. Comparison figures of exact solutions (left) and approximation solutions (right) with $N = 30$ and $M = 15$.

As shown in Tables 1-2, the errors decline quickly with the increase of N and M. When $N \geq 30, M \geq 12$, the approximate solutions achieve at about 10^{-12} accuracy. We further observe from Figures 1-4 that our algorithm is convergent and highly accurate. In addition, to test the spectral accuracy of our algorithm,

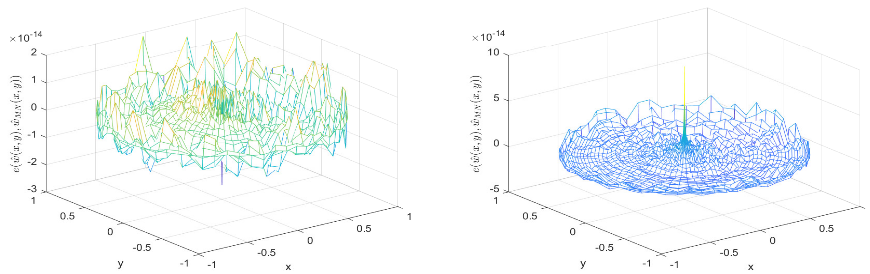

Figure 2. The error figures of exact solutions $\hat{w}(x, y)$ and approximation solutions $\hat{w}_{MN}(x, y)$ with $N = 30$ and $M = 14$ (left) and $N = 45$ and $M = 25$ (right).

Table 2. The error $e(\hat{u}(x, y), \hat{u}_{MN}(x, y))$ between approximate solutions and exact solutions for different M and different N.

N	$M = 4$	$M = 8$	$M = 12$	$M = 16$
20	7.3633e-05	1.6825e-09	1.5424e-08	9.4362e-05
25	7.3689e-05	1.6797e-09	1.9860e-14	6.3512e-10
30	7.4222e-05	1.6790e-09	1.0061e-14	1.1102e-15
35	7.4567e-05	1.6892e-09	1.0013e-14	1.5543e-15

we also present the corresponding error curves between the numerical solutions and exact solutions on log-log scale in Figure 5. It can be observed from Figure 5 that the error converges to zero exponentially.

Example 7.2. We take $R = 1$, $\hat{u} = (x^2+y^2-1)^3 sin((x+y)\pi)$. By plugging $\hat{u}(x, y)$ into equations (2.1)-(2.3), we can obtain $\hat{f}(x, y), \hat{\varphi}(x, y)$ and $\hat{\psi}(x, y)$. For different N and M, the errors between approximate solutions and exact solutions are listed in Tables 3-4. To further demonstrate the efficiency and accuracy of our algorithm, we draw the images of the exact solutions and the approximate solutions in Figures 5 and 7 and the error images between them in Figures 6 and 8.

We see from Tables 3-4 that the approximate solutions also achieve at about 10^{-12} accuracy with $N \geq 30, M \geq 12$. We further observe from Figures 6-9 that

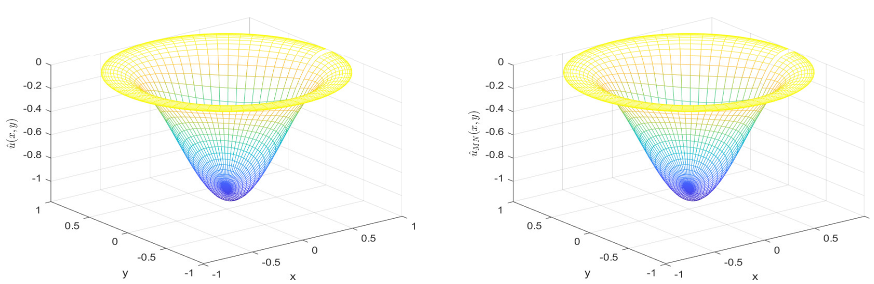

Figure 3. Comparison figures of exact solutions (left) and approximation solutions (right) with $N = 35$ and $M = 15$.

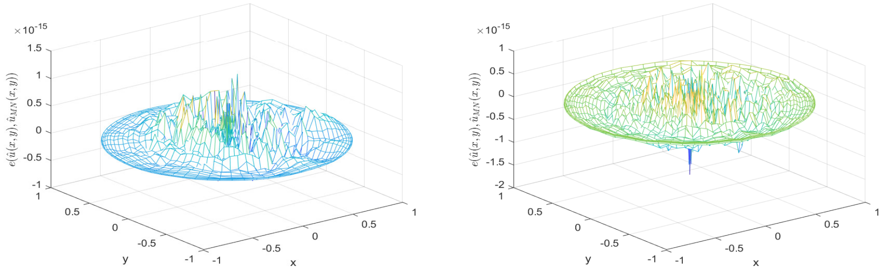

Figure 4. The error figures of exact solutions $\hat{u}(x,y)$ and approximation solutions $\hat{u}_{MN}(x,y)$ with $N = 30$ and $M = 15$ (left) and$N = 45$ and $M = 25$ (right).

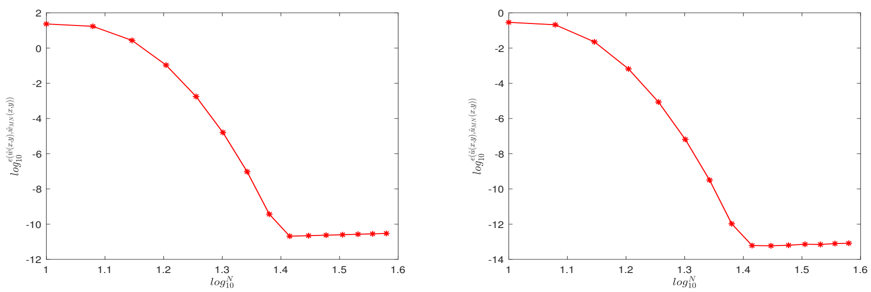

Figure 5. Error curves between the numerical solutions $\hat{w}_{MN}(x,y)$ (left) and $\hat{u}_{MN}(x,y)$(right) and their exact solutions on log-log scale with different N and $M = 12$.

Table 3. The error $e(\hat{w}(x,y), \hat{w}_{MN}(x,y))$ between approximate solutions and exact solutions for different M and different N.

N	$M = 4$	$M = 8$	$M = 12$	$M = 16$
20	0.0061	3.1825e-07	2.4694e-07	0.0023
25	0.0060	3.1166e-07	6.9387e-12	1.5468e-07
30	0.0061	3.1801e-07	3.4162e-12	1.2434e-14
35	0.0061	3.1590e-07	3.4337e-12	1.2434e-14

Table 4. The error $e(\hat{u}(x,y), \hat{u}_{MN}(x,y))$ between approximate solutions and exact solutions for different M and different N.

N	$M = 4$	$M = 8$	$M = 12$	$M = 16$
20	6.3773e-05	1.4955e-09	1.1306e-09	1.1503e-05
25	6.3807e-05	1.5017e-09	1.9439e-14	6.0945e-10
30	6.3829e-05	1.4920e-09	9.3085e-15	2.7756e-16
35	6.3845e-05	1.5073e-09	9.1524e-15	2.7756e-16

our algorithm is also convergent and highly accurate.

Example 7.3. We consider the eigenvalue problem (6.1)-(6.3). Here, setting $R = 2$,

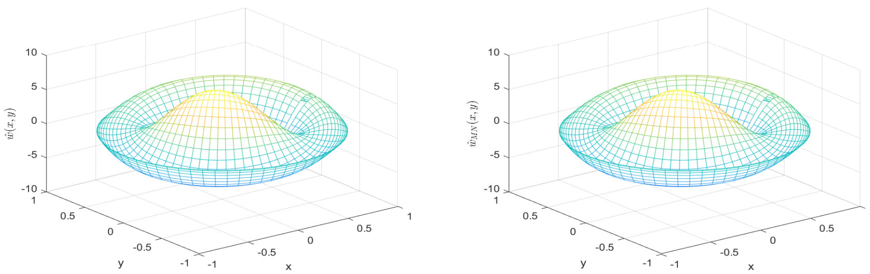

Figure 6. Comparison figures of exact solutions (left) and approximation solutions (right) with $N = 35$ and $M = 15$.

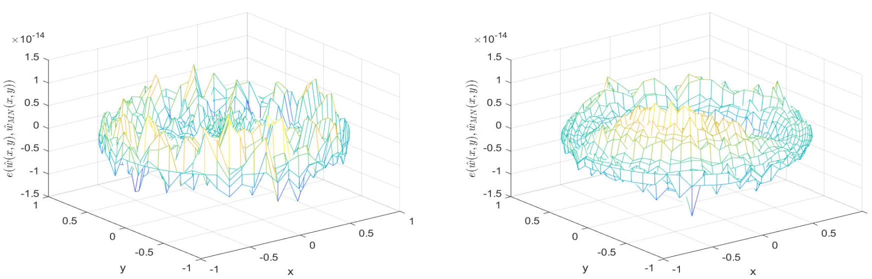

Figure 7. The error figures of exact solutions $\hat{w}(x, y)$ and approximation solutions $\hat{w}_{MN}(x, y)$ with $N = 30$ and $M = 14$ (left) and$N = 35$ and $M = 15$ (right).

$\alpha = 0$ and $\beta = 1$. The numerical results of the first four approximate eigenvalues for different m and N are listed in Tables 5 and 6, respectively.

We observe from Tables 5 and 6 that the first four numerical eigenvalues achieve about 13-digit accuracy when $N \geq 20$. In order to show the spectral accuracy of our algorithm intuitively, we take numerical solutions of $N = 60$ as the reference solutions λ_{ref} and plot the error tendency curves in Figure 10. Here the error is defined as $|\lambda^i_{mN} - \lambda_{ref}|$ $(i = 1, 2, 3, 4,\ m = 0, 1)$. In addition, we also present the corresponding error curves on log-log scale in Figure 11. It can be observed from Figures 10-11 that all the first four numerical eigenvalues converge exponentially.

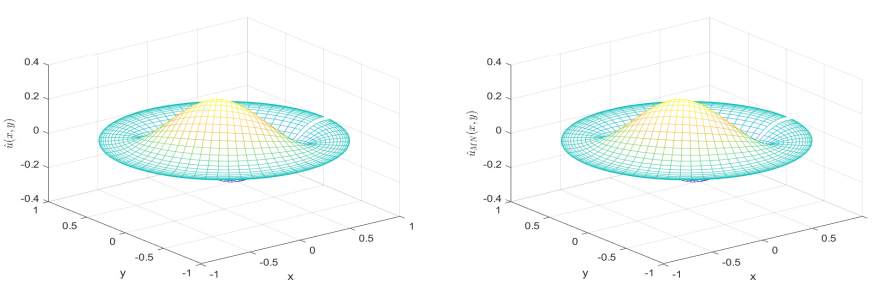

Figure 8. Comparison figures of exact solutions (left) and approximation solutions (right) with $N = 35$ and $M = 15$.

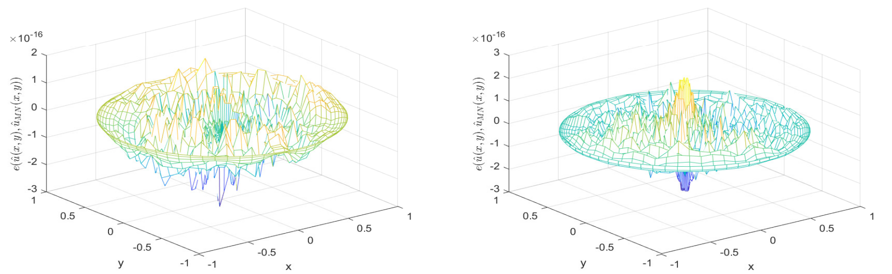

Figure 9. The error figures of exact solutions $\hat{u}(x,y)$ and approximation solutions $\hat{u}_{MN}(x,y)$ with $N=30$ and $M=14$ (left) and $N=40$ and $M=25$ (right).

Table 5. Numerical results of the first four eigenvalues for different N when $m=0$.

N	λ_{0N}^1	λ_{0N}^2	λ_{0N}^3	λ_{0N}^4
10	3.090327492626542	59.031114309908325	351.5037169220989	1209.444613357836
15	3.090327492626550	59.031114301017460	351.5039866293564	1209.262543205556
20	3.090327492626549	59.031114301017470	351.5039866293499	1209.262543336919
25	3.090327492626535	59.031114301017150	351.5039866293507	1209.262543336922
30	3.090327492626531	59.031114301017354	351.5039866293507	1209.262543336927

Table 6. Numerical results of the first four eigenvalues for different N when $m=1$.

N	λ_{1N}^1	λ_{1N}^2	λ_{1N}^3	λ_{1N}^4
10	14.472516371010260	152.4035296249379	670.5003418074672	1972.379885614160
15	14.472516371011748	152.4035276681599	670.5085597879880	1970.601410053427
20	14.472516371011745	152.4035276681601	670.5085597869706	1970.601415635077
25	14.472516371011760	152.4035276681600	670.5085597869690	1970.601415635074
30	14.472516371011720	152.4035276681597	670.5085597869692	1970.601415635074

Example 7.4. We still consider the eigenvalue problem (6.1)-(6.3). Here, setting $R=3$, $\alpha=1$ and $\beta=3$. The numerical results of the first four approximate eigenvalues for different m and N are listed in Tables 7 and 8, respectively.

Table 7. Numerical results of the first four eigenvalues for different N when $m=0$.

N	λ_{0N}^1	λ_{0N}^2	λ_{0N}^3	λ_{0N}^4
10	4.055480414179577	17.848631976203723	80.556077439014260	257.1551932387490
15	4.055480414179569	17.848631974188100	80.556133915876060	257.1180648278905
20	4.055480414179572	17.848631974188190	80.556133915875050	257.1180648546771
25	4.055480414179571	17.848631974188110	80.556133915875110	257.1180648546774
30	4.055480414179525	17.848631974187555	80.556133915875210	257.1180648546775

We observe from Tables 7 and 8 that the first four approximate eigenvalues achieve about 14-digit accuracy when $N \geq 20$. Similarly, in order to show the

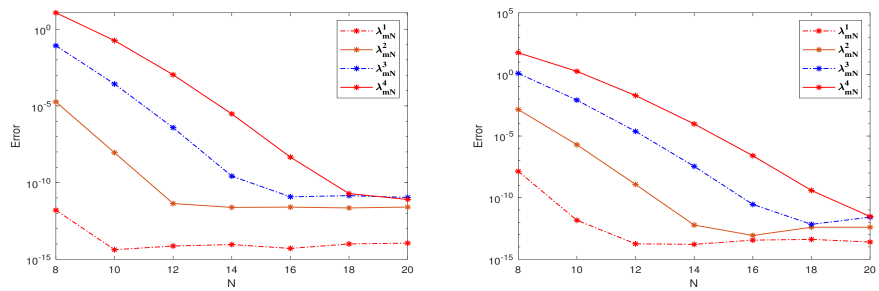

Figure 10. The error tendency curves between numerical solutions and reference solutions with $m = 0$ (left) and $m = 1$ (right).

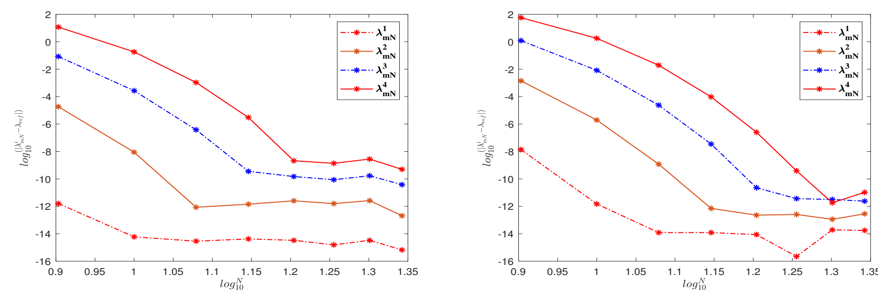

Figure 11. Errors between the numerical solutions and the reference solutions on log-log scale with $m = 0$ (left) and $m = 1$ (right).

Table 8. Table 8 Numerical results of the first four eigenvalues for different N when $m = 1$.

N	λ^1_{1N}	λ^2_{1N}	λ^3_{1N}	λ^4_{1N}
10	7.292567873028044	38.375587453787304	146.7468498404038	412.1418053276755
15	7.292567873028434	38.375587031923580	146.7485437242564	411.7815982705580
20	7.292567873028433	38.375587031923594	146.7485437240460	411.7815994010555
25	7.292567873028427	38.375587031923560	146.7485437240464	411.7815994010549
30	7.292567873028430	38.375587031923660	146.7485437240463	411.7815994010551

spectral accuracy of our algorithm intuitively, we take numerical solutions of $N = 60$ as the reference solutions λ_{ref} and plot the error tendency curves in Figure 12. Here the error is still defined as $|\lambda^i_{mN} - \lambda_{ref}|$ $(i = 1, 2, 3, 4,\ m = 0, 1)$. Obviously, Figure 12 indicates that all the first four numerical eigenvalues are converge exponentially.

8. Conclusion

We have presented in this paper a highly accurate numerical method for the fourth-order problems with simply supported plate boundary conditions. The novelty of this paper has three main points: (1) We reduce the fourth-order problem to a coupled second-order problem, which overcomes the complexity of constructing basis functions. (2) We use dimension reduction technique to decompose the cou-

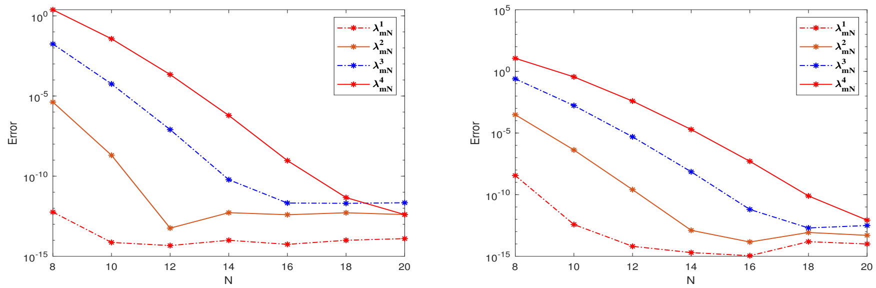

Figure 12. The error tendency curves between numerical solutions and reference solutions with $m = 0$ (left) and $m = 1$ (right).

pled second-order problem into the one-dimensional coupled second-order problem, which not only overcomes the complexity of the curved domain, but also greatly reduces the degree of freedom of calculation. (3) We give a rigorous error analysis for the proposed algorithm. In addition, some numerical examples are given, and the numerical results verify the effectiveness of the algorithm and the correctness of the theoretical results. Note that the approaches developed in this paper can be extended to more complex domains(such as L-shaped domain, spherical domain, and so on) by using spectral element methods or finite element methods.

References

[1] S. Abbasbandy, E. Shivanian, K. H. AL-Jizani, et al., *Pseudospectral meshless radial point interpolation for generalized biharmonic equation subject to simply supported and clamped boundary conditions*, Engineering Analysis with Boundary Elements, 2021, 125, 23–32.

[2] J. An, H. Li and Z. Zhang, *Spectral-Galerkin approximation and optimal error estimate for biharmonic eigenvalue problems in circular/spherical/elliptical domains*, Numerical Algorithms, 2020, 84(2), 427–455.

[3] J. An and Z. Zhang, *An efficient spectral-Galerkin approximation and error analysis for Maxwell transmission eigenvalue problems in spherical geometries*, Journal of Scientific Computing, 2018, 75(1), 157–181.

[4] W. Bao, L. Chen, X. Jiang, et al., *A Jacobi spectral method for computing eigenvalue gaps and their distribution statistics of the fractional Schrödinger operator*, Journal of Computational Physics, 2020, 421(15), 109733.

[5] C. Canuto, *Eigenvalue approximations by mixed methods*, RAIRO. Analyse NuméRique, 1978, 12(1), 27–50.

[6] L. Chen, J. Shen and C. Xu, *A triangular spectral method for the Stokes equations*, Numerical Mathematics: Theory, Methods and Applications, 2011, 42, 158–179.

[7] W. Chen and Q. Lin, *Approximation of an eigenvalue problem associated with the stokes problem by the stream function-vorticity-pressure method*, Applications of Mathematics, 2006, 51(1), 73–88.

[8] G. Engel, K. Garikipati, T. Hughes, et al., *Continuous/discontinuous finite element approximations of fourth-order elliptic problems in structural and con-*

tinuum mechanics with applications to thin beams and plates, and strain gradient elasticity, Computer Methods in Applied Mechanics and Engineering, 2002, 191(34), 3669–3750.

[9] F. Haddouchi and N. Houari, *Monotone positive solution of fourth order boundary value problem with mixed integral and multi-point boundary conditions*, Journal of Applied Mathematics and Computing, 2021, 66, 87–109.

[10] D. Kaur and R. K. Mohanty, *Highly accurate compact difference scheme for fourth order parabolic equation with Dirichlet and Neumann boundary conditions: Application to good Boussinesq equation*, Applied Mathematics and Computation, 2020, 378, 125202.

[11] B. Li, G. Fairweather and B. Bialecki, *Discrete-time orthogonal spline collocation methods for vibration problems*, *SIAM Journal on Numerical Analysis*, 2002, 39, 2045–2065.

[12] L. Li and J. An, *An efficient spectral method and rigorous error analysis based on dimension reduction scheme for fourth order problems*, Numerical Methods for Partial Differential Equations, 2021, 37(1),152–171.

[13] Y. Ma and L. Chen, *A Jacobi-Galerkin spectral method for computing the ground and first excited states of the nonlinear fractional Schrödinger equation*, East Asian Journal on Applied Mathematics, 2020, 10(2), 274–294.

[14] M. Molina-Meyer and F. R. Prieto-Medina, *Pseudospectral versus Galerkin methods: Fourth order equations*, Journal of Computational and Applied Mathematics, 2022, 413, 114348.

[15] J. Rappaz, B. Mercier, J. Osborn, et al., *Eigenvalue approximation by mixed and hybrid methods*, Mathematics of Computation, 1981, 36(154), 427–453.

[16] S. Ren, T. Tan and J. An, *An efficient spectral-Galerkin approximation based on dimension reduction scheme for transmission eigenvalues in polar geometries*, Computers and Mathematics with Applications, 2020, 80(5), 940–955.

[17] J. Shen, *Efficient spectral-Galerkin methods III: Polar and cylindrical geometries*, Journal on Scientific Computing, 1997, 18(6), 1583–1604.

[18] J. Shen, *Efficient spectral-Galerkin methods IV. Spherical geometries*, Journal on Scientific Computing, 1999, 20(4), 1438–1455.

[19] J. Shen and J. An, *Spectral approximation to a transmission eigenvalue problem and its applications to an inverse problem*, Computers and Mathematics with Applications, 2015, 69(10), 1132–1143.

[20] J. Shen and T. Tang, *Spectral Methods: Algorithms, Analysis and Applications*, Science Press, 2006.

[21] J. Shen, T. Tang and L. Wang, *Spectral Methods: Algorithms, Analysis and Applications*, Springer Science in Computational Mathematics, 2011, 41. Springer, Heidelberg.

[22] J. Shen, L. Wang and H. Li, *A triangular spectral element method using fully tensorial rational basis functions*, Journal on Numerical Analysis, 2009, 47(3), 1619–1650.

[23] J. Shen, J. Xu and J. Yang, *The scalar auxiliary variable (SAV) approach for gradient flows*, Journal of Computational Physics, 2018, 353, 407–416.

[24] J. Shen, J. Xu and J. Yang, *A new class of efficient and robust energy stable schemes for gradient flows*, *SIAM Review*, 2019, 61(3), 474–506.

[25] E. Shivanian and S. Abbasbandy, *Pseudospectral meshless radial point interpolation for generalized biharmonic equation in the presence of Cahn-Hilliard conditions-*, Computational and Applied Mathematics, 2020, 39, 1–18.

[26] T. Tan, W. Cao and J. An, *Spectral approximation based on a mixed scheme and its error estimates for transmission eigenvalue problems*, Computers and Mathematics with Applications, 2022, 111, 20–33.

[27] Y. Yang and W. Jiang, *Upper spectral bounds and a posteriori error analysis of several mixed finite element approximations for the stokes eigenvalue problem*, Science China Mathematics, 2013, 56(6), 1313–1330.

[28] B. Zinsou, *Asymptotics of the eigenvalues of self-adjoint fourth order boundary value problems*, Differential Equations and Dynamical Systems, 2021, 1–22.